Ion Transport in Cesium Lead Halide Perovskites

A Thesis

submitted to
Indian Institute of Science Education and Research Pune
in partial fulfillment of the requirements for the
BS-MS Dual Degree Programme

by

Danish Kaur Pannu
20141143

Indian Institute of Science Education and Research Pune
Dr. Homi Bhabha Road,
Pashan, Pune 411008, INDIA.

April, 2019

Supervisor: Dr. Mukul Kabir

Certificate

This is to certify that this dissertation entitled Ion Transport in Cesium Lead Halide Perovskites towards the partial fulfilment of the BS-MS dual degree programme at the Indian Institute of Science Education and Research, Pune represents study/work carried out by Danish Kaur Pannu at Indian Institute of Science Education and Research under the supervision of Dr. Mukul Kabir, Department of Physics , during the academic year 2018-2019.

Dr. Mukul Kabir

Committee:

Dr. Mukul Kabir

Dr. Prasenjit Ghosh

This thesis is dedicated to my grandparents.

Declaration

I hereby declare that the matter embodied in the report entitled Ion Transport in Cesium Lead Halide Perovskites are the results of the work carried out by me at the Department of Physics, Indian Institute of Science Education and Research, Pune, under the supervision of Dr. Mukul Kabir and the same has not been submitted elsewhere for any other degree.

Danish Kaur Pannu

Acknowledgments

First and foremost, I want to express my gratitude towards my supervisor, Dr. Mukul Kabir, whose constant support kept me motivated throughout the duration of my master's thesis project. I particularly found discussions with him very insightful and valuable. He has always taken out the time to talk to me when I needed it, be it for academic and non-academic advice, for motivation or for encouragement.

Next, I would like to thank my research group members, Rohit Babar, Chandan Singh, Bhagyashri Bhat, Srilatha Arra and Deepak Kumar Roy. They have always been there to clear my doubts and discuss new ideas. I thoroughly enjoyed and greatly value the time spent with them.

There are some teachers at IISER, apart from my supervisor, who played a crucial role in developing my interest in condensed matter physics, namely, Dr. Ashna Bajpai, Dr. Prasenjit Ghosh and Prof. Satish Ogale.

I especially want to thank Dr. Bhas Bapat, with whom I have had a lot of discussions about education, and who has encouraged me to pursue what I really enjoy and provided me with opportunities to do so.

I am very grateful to my friends, Suman, Nandini, Shweta and Dhriti for motivating me in times when I needed it; Anwesh and Nandu for constantly reminding me that there are ample opportunities for me; Mayank, Lakshmi, Megha, Rasika, Rohit, Tathagata, Aditya and Priya, for their sweet gestures of encouragement; Tomin, Dhriti, Aanjaneya and John for refreshing conversations. I also want to thank my comrades from theatre, who have been sources of joy and inspiration in the last five months at IISER. Especially, Abhinav and Achintya who have been brilliant at assisting me in working for our theatre production,

thereby reducing my workload so that I can focus on my thesis.

I thank my mum, who is always there through thick and thin, my dad, who always helps me put things in perspective and my brother, just because he's a part of the family (and maybe, for gifting me an iPad).

Lastly, it would not have been possible to write this thesis without the constant support of my friend in the most crucial time of its genesis - Bart, thank you.

Abstract

Perovskite solar cells have gained a great deal of attention in the energy research community, both in academia and industry. They are considered as promising candidates for replacing existing commercial solar cells, given their high efficiency (up to 23%) and simple, cost effective synthesis. However, there are still numerous challenges for their commercialisation. The two major issues are their short lifetimes and hysteresis in their current-voltage curve. This thesis aims at studying ion transport in perovkites, which is considered as the culprit behind these problems. Very little is known about the exact mechanism of ion transport in perovskites and there exist conflicting results in literature about its relation to perovskite solar cell efficiencies.

Through this thesis, we aim at resolving some of the ambiguities revolving around ion transport by discussing its dependence on phase of crystal and the type of ion in the perovskite. In this regard, we have found, using nudged elastic band method, the activation energy barriers for transport of halide ions, mediated by vacancy defects, in cesium halide perovskites ($CsPbX_3$, X = Cl, Br, I) for different crystal phases. Our study is important for futher understanding of perovskites because there is no existing literature on dependency of ion transport on phases of perovskites.

Our results show that the activation energy barriers for ionic transport in orthorhombic phases (which exist at room temperature) are lower than the barriers for cubic phases, indicating that the ions are more stable in cubic phase. However, interestingly, the vacancy formation energy for cubic phase is lower. These results have been compared with experimental values of activation energies.

We have also found the diffusivity of ions at different temperatures, which is found to be of the order of $10^{-8} - 10^{-9} cm/s^2$ around room temperature (300K). To put things in perspective, the diffusion coefficient of intrinsic semiconductors, such as Si, Ge, As, are of the order of $10^{-13} cm/s^2$ at temperatures as high as 1200K. Hence, perovskites have relatively higher levels of diffusion even at room temperatures.

The work presented in this thesis can be useful for further studies of ion migration in perovskites and help in predicting more stable perovskite structures for the purposes of photovoltaics.

Contents

List of Tables

List of Figures

Chapter 1

Introduction

Our planet is facing a serious threat due to rapid global warming and climate change[1]. The biggest factor contributing to this change is fossil fuel emissions[17]. Additionally, fossil fuels are non-renewable resources and are soon going to deplete. Hence, it is high time that we completely switch to alternate energy sources which are environment friendly, renewable and sustainable. Out of the available renewable energy resources, solar energy has an edge over others because of its universal availability, low cost, no requirement of distribution infrastructure and minimal maintenance[8]. Furthermore, electricity generation by solar energy using photovoltaics has almost zero environmental impact beyond device manufacturing. Having efficient methods to utilise this resource would basically opening the doors to unlimited clean energy at a very low price. Although, there has been a rapid growth in solar power generation in the past few years, its overall share in the global energy generation is still as low as 1.7%.

Ever since the first silicon solar cell was manufactured in 1941 by Bell Labs[36][35], there have been tremendous efforts made to manufacture more efficient and less expensive photovoltaics (PVs) all over the world. The first generation PVs are based on crystalline silicon which require high temperatures for manufacturing and the resulting residual waste is harmful to the environment. The second generation PVs are based on thin film inorganic compounds such as a-Si:H (hydrogenated amorphous silicon), CdTe (cadmium telluride), and CIGS (copper indium gallium selenide). Often, their thin film preparation requires vacuum

[1]Over 97% of the peer-reviewed research papers published by climate scientists endorse anthropogenic global warming, i.e., global warming at the current rate is being caused by human activities.

vapour deposition method that consumes high energy. Next, there are the third generation PV technologies, which are solution processed thin film solar cells. They are specially designed to generate high power conversion efficiency (PCE) at low device fabrication cost; these include light condensed cells, organic photovoltaic cell (OPV), dye-sensitized solar cells (DSSCs) and perovskite solar cells (PVCs).

1.1 Perovskite structure

In the year 1839, Gustav Rose (1798-1893), a German mineralogist, discovered a calcium titanium oxide ($CaTiO_3$) mineral in the Ural Mountains of Russia which was named "perovskite" in honour of a Russian mineralogist, Lev Perovski (1792-1856). The perovskite structure gained significant attention due to its stable geometry.

The general formula of a perovskite is ABX_3, where A and B are cations, A being bigger than B, and X is an anion, usually oxygen or halogen.

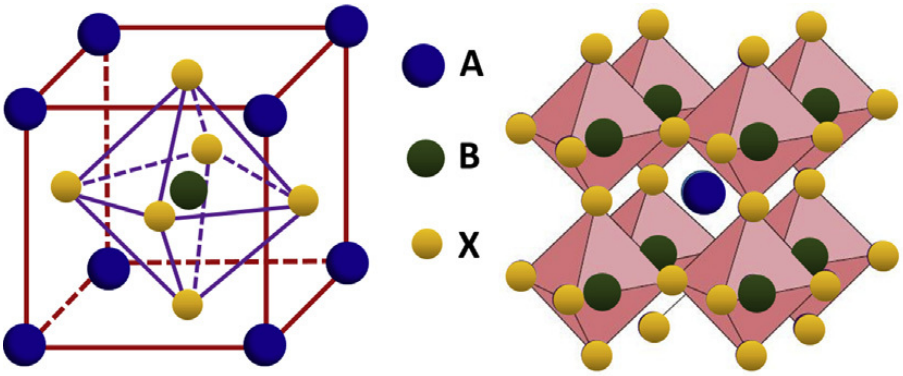

Figure 1.1: The ideal perovskite structure is a cubic closed packed structure with cation B enclosed in an octahedral formed by X ions. Cation A sits at the centre of eight such octahedrals. Picture taken from [57]

Tolerance factor and Octahedral factor

In reality, perovskites somewhat deviate from their ideal structure as the octahedrals distort to give different phases. This depends on the sizes of A,B and X ions. Depending on the tolerance factor, t, and octahedral factor, μ, (defined below), one can roughly determine how

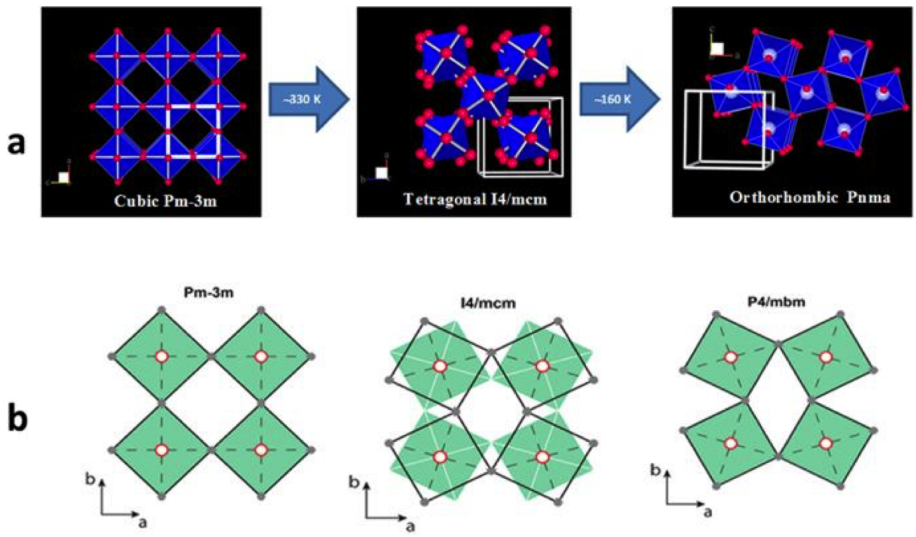

Figure 1.2: The range of the tolerance factor is usually between 0.89 and 1.00 for oxide perovskites and between 0.85 to 1.11 for halide perovskites[27] Picture taken from [53]

geometrically stable the perovskite structure is.

$$t = \frac{R_A + R_X}{\sqrt{2}(R_A + R_B)} \quad ; \quad \mu = \frac{R_X}{R_B} \tag{1.1}$$

Here, R_A, R_B and R_X are radii of atom A, B and X respectively. If $t = 1$, the perovskite is in perfect cubic phase. As t moves away from 1, the structure goes from cubic to tetragonal and then towards orthorhombic phase. The tolerance factor gives the measure of the octahedral tilting and the octahedral factor gives the ratio of radii of cation B and anion X. For $\mu > 0.422$, a halide perovskite structure would form[42]. Below this value, the BX_6 octahedron will become unstable and the perovskite structure will not be formed.

Perovskites exist in mainly three different phases - cubic, tetragonal and orthorhombic. Phase transition occurs with decrease in temperature from cubic to tetragonal and from tetragonal to orthorhombic.

1.2 Perovskite solar cells

Perovskites have emerged as promising candidates for the light harvesting layer of solar cells in the past decade with their efficiencies increasing at a rapid rate from 3.8% in 2009[24] to

23.7% at present[2] [21][34] (see Fig. 1.3).

Furthermore, unlike other photovoltaic technologies, perovskites don't require complex manufacturing procedures or high cost equipment for their production. They can be synthesised using simple coating techniques at room temperature. Despite having high efficiencies and low-cost production with minimal technological sophistication, PSCs have major barriers to cross before they can be commercialised[43][18][7]. The two major concerns that are being extensively addressed are 1) rapid degradation of PSCs and 2) hysteresis in their photocurrent-voltage curve. Resolving these two problems would result in a revolutionary step towards sustainable energy development.

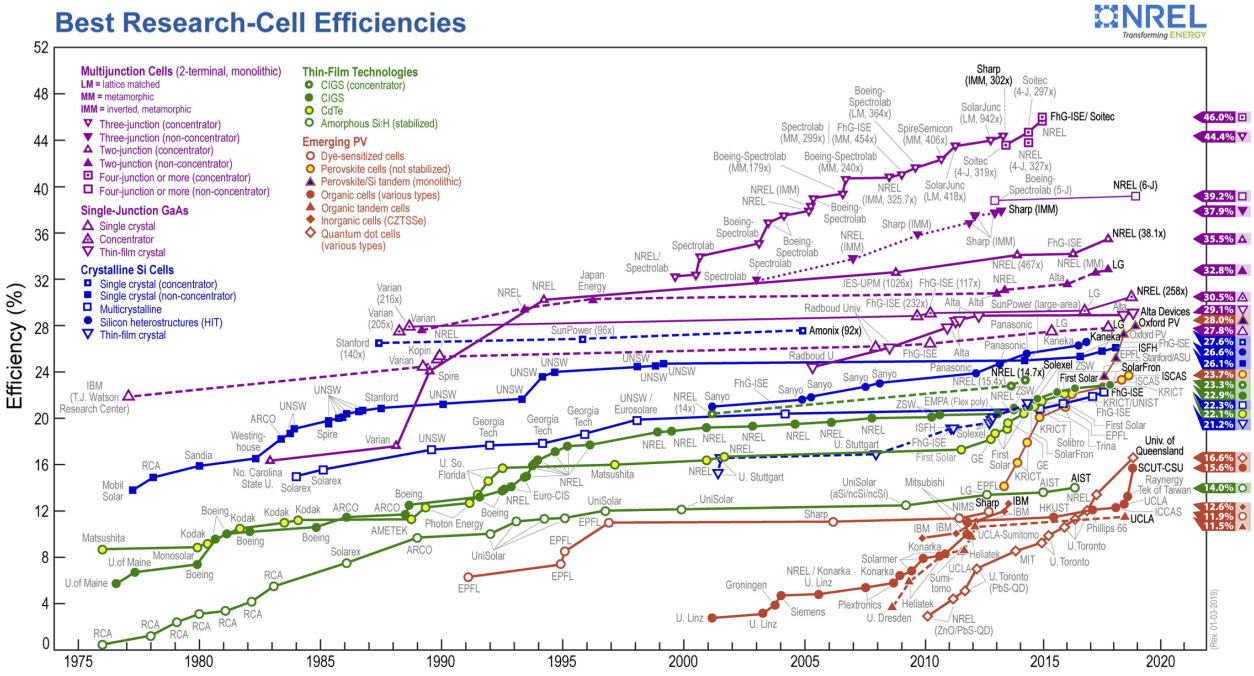

Figure 1.3: Maximum power conversion efficiencies (PCE) of various photovoltaic cells since 1976. The PCEs of perovskites and perovskite/Si tandem cells have grown fastest out of all the photovoltaics. However, perovskite cells are still not stable enough for commercial use. Picture taken from NREL (National Renewable Energy Laboratory) [34].

1.2.1 Stability

The maximum lifetime of PSCs on record is one year[12], which is not comparable to the 25 year-long lifetime of Si based cells. Furthermore, most of the perovskite based solar cells

[2]Recently, Oxford PV^{TM} developed perovskite-silicon tandem solar cells with 27.3% efficiency.[1]

degrade within a few weeks, making them unavailable for commercial use as of now. Many efforts have been made to understand the instability issues related to PSCs[30]. Extrinsic factors that degrade these materials include moisture, oxygen, illumination and external electric field. These can be taken care of, to a large extent, by encapsulating the solar cell in a protective layer. However, intrinsic factors that affect the stability of PSCs are more difficult to tackle. These include thermal instability (structural distortion or phase transition due to temperature change) and ion migration[30]. Out of these, ion migration is more troublesome because it can't be avoided given that the solar cell is always under some external potential and perovskites are known to have ionic conductance[40].

1.2.2 Hysteresis in J-V curve

Another concern about PSCs is the existence of hysteresis in their photocurrent density-voltage (J-V) curve[6][49], which results in depletion of their efficiencies over time. This hysteric behaviour is attributed to various processes including ferroelectricity, charge trapping/detrapping and ion migration[40]. It has been widely agreed that ion migration is the more dominant factor out of these three.

Hence, the two major challenges for evolution of the PSC technology, stability and hysteresis, are attributed to ion migration. However, there is not enough theoretical understanding about the mechanism of ion migration within perovskites.

1.3 Inorganic lead halide perovskites

Currently, the best candidate for cation B is Pb, having the maximum power conversion efficiency amongst all perovskites so far. Zhang et. al. [56] have discussed the reasons behind the special stature of lead. The reasons that they have given are as follows:

> (i) a strong and quickly-rising direct-gap optical transition between the valence Pb_s/X_p and conduction Pb_p states, (ii) a small exciton binding energy, (iii) low effective masses of both electrons and holes, (iv) energetically shallow intrinsic defect levels, beneficial for bipolar conductivity and meanwhile minimizing carrier

trapping and scattering, and (v) suitability of low-cost, non-vacuum solution routes for film deposition.

Therefore, ample literature is available on lead halide perovskite cells. Extensive studies have been conducted on lead halide perovskites as solar harvesters and it has been established that while organic-inorganic hybrid perovskites (e.g. $MAPbX_3$) have a more stable geometry, due to the larger organic cation sitting in the octahedron, as compared to inorganic perovskites (e.g. $CsPbX_3$), the latter are found to be thermodynamically more stable than their hybrid counterparts[3][48]. Zhou et al. showed that while Cs-based perovskites retained >99% of their efficiency after continued illumination for 1500 hours, $CH_3NH_3PbI_3$ perovskites degraded rapidly after 50 hours of exposure[58]. Therefore, recently, there has been a shift towards inorganic perovskites from hybrid organic-inorganic perovskites.

Hence, we have chosen to work on Cs-based inorganic lead halide perovskites for this project.

Material	Temperature (°C)		
	Orthorhombic	Tetragonal	Cubic
$CsPbCl_3$[15]	T<42	42<T<47	T>47
$CsPbBr_3$[16]	T<88	88<T<130	T>130
$CsPbI_3$[50]	T<290	290<T<316	T>316

Table 1.1: Different phases of $CsPbX_3$ with respect to temperature.

The approximate temperature range which a solar cell has to bear is -20°C to 80°C[19]. Hence, perovskites need to be stable in this temperature range and not undergo any phase transition. From the Table 1.1, it is evident that $CsPbCl_3$ is not suited for this purpose, unless we stablize its structure (by doping perhaps) in this range. Furthermore, since the temperature range of the tetragonal phase of $CsPbCl_3$ is very narrow, it is almost never observed in nature and is extremely difficult to obtain in lab. For this reason, we have not considered this phase for further calculations.

[3]The geometry of the inorganic perovskites can be made better by putting more than one A cations in place of just one. These are called double/triple perovskites.

1.4 Ion migration in perovskites

Let us now have a look at the various ways of ion transport within halide perovskites and the possible effects it can have on the crystal lattice. Fig. 1.4 shows the possible pathways through which ions can move in a crystal. These include Schottky (vacancy) defects, Frenkel defects, lattice distortion by accumulated charges and dissolved impurities, through channels in grain boundaries, and because of strain induced by external electric field and illumination. Vacancy mediated ion transport has been considered in this project as these defects are expected to have lower activation energies as compared to other local defects.

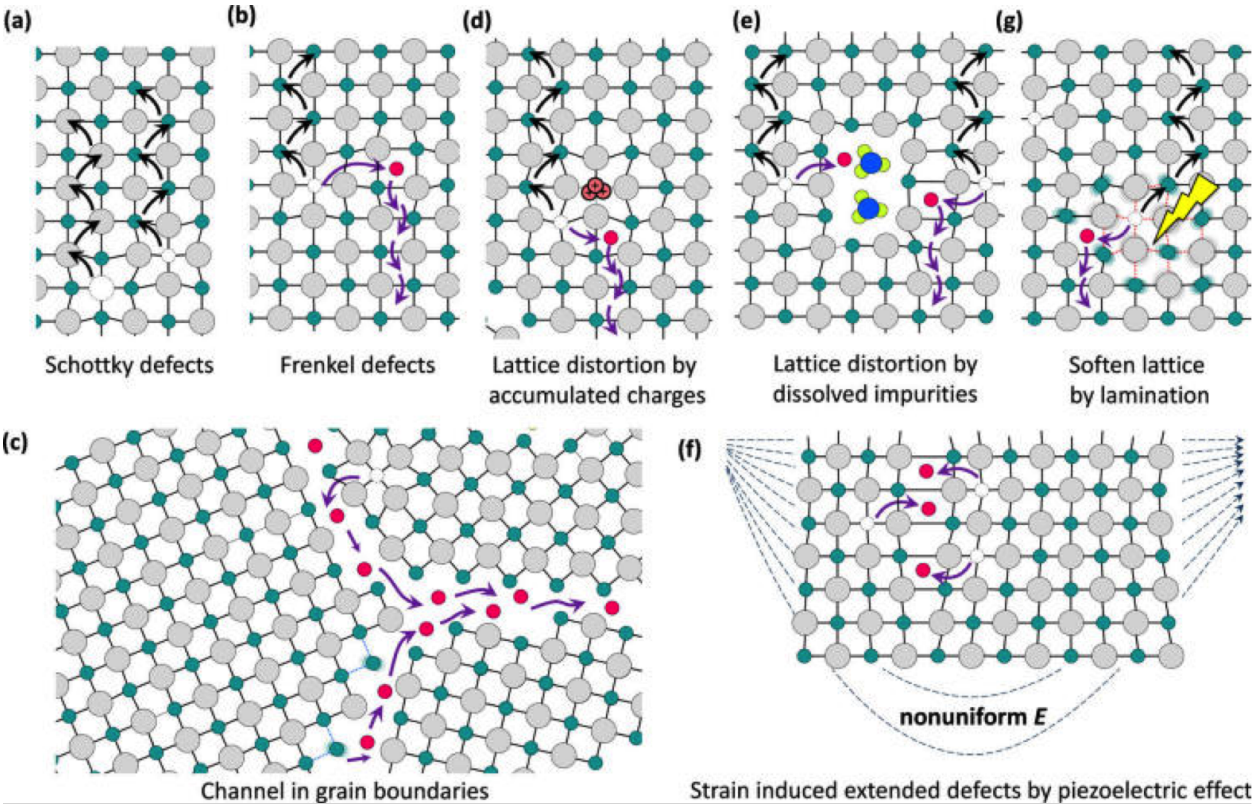

Figure 1.4: There are many pathways for ion migration. The easiest path for ions to migrate is through grain boundaries, since the surface ions have comparatively lesser binding forces. Picture taken from [55]

In cesium lead halides, out of Cs^{+}, Pb^{2+} and X^{-} ions, Pb^{2+} is expected to have highest activation energy for transport, given that 1) it has higher charge, so the binding energy would be more and 2) it is caged inside the PbX_6 octahedron, so transport to another site would be difficult. Additionally, severeal computational studies have been conducted to find activation energies of ions in hybrid halide perovskites and it has been found that E_a for

halide ions is much lower than E_a for the cations (MA, FA, Pb)[38] We have made the same assumption for inorganic halide perovskites.

Despite several studies on ion migration in perovskites, its exact mechanism is still not understood. Conflicting results have been reported about the the role of ion migration in affecting efficiencies of perovskite solar cells. Tsai H. et al reported that lattice expansion due to illumination leads to higher efficiencies of mixed-cation halide perovskite device[51]. On the other hand, movement of charged ions can inhibit electron and hole collection at electrode contacts[45] resulting in hysteresis, which negatively affects the efficiency of PSCs.It has also has been shown that introduction of Cl in synthesis of $MAPbI_3$ perovskites enhances the device performance[28]. Domanski K et. al. showed that the migration of cations in perovskites, which happens over timescales of minutes or hours[4] reduces the initial efficiency by 10-15% after several hours of operation. However, on leaving the device in the dark for comparable amount of time, the initial efficiency is fully recovered[9]. All these observations indicate that there is some role of ion diffusion in deciding performance of perovskites as solar cells.

Therefore, studying ion transport within perovskite crystals is crucial in further advancement of PSCs. In this project, we have studied halide ion transport due to vacancy defects in cesium lead halide perovskites.

[4]Halide ions on the other hand migrate over timescales much lesser than this, i,e, from 10^{-1} to 100 s.

Chapter 2

Theoretical Framework and Methodology

In this chapter, I have elaborated on the theoretical concepts that have been used in this thesis. This includes discussion of ion diffusion in solids, in particular, Fick's laws and calculation of diffusivity using jump frequency. Emphasis has been put on solving many-body Hamiltonion using Density Functional Theory and various exchange-correlation functionals that can be used to approximate the interaction between electrons. The Kohn-Sham scheme wherein an interacting system of particles is mapped to a non-interacting one, has been explained in detail. Thereafter, the self-consistent iterative numerical method to find ground state energies of many-body systems has been stated. Additionally, I have discussed the nudged elastic band method, which is used to calculate activation energy barriers for ion transport. In the last section, I have discussed the computational methods used in this project.

2.1 Ionic diffusion in solids

The theory of diffusion in solids was majorly developed in mid-1900s with contributions from pioneers like Arrhenius, Fick, Einstein and Wigner[29]. In this section, the basic theory of diffusion has been discussed, with special attention to diffusion due to vacancy defects in solids. For my systems, I have made the assumption that diffusion is happening in isotropic

conditions and only nearest neighbour transport is looked at. The following Fick's laws hold for these conditions.

2.1.1 Fick's Laws of Diffusion

Fick's First Law

This is an empirical law which states that the flux of the diffusion of particles in a particular direction is directly proportional to the change in concentration of those particles along that direction. For a one dimensional flow, this can be written as:

$$J_x = -D\frac{\partial C}{\partial x} \tag{2.1}$$

where J_x is the flux of particles in x direction (diffusion flux), i.e. the number of particles passing a unit area (perpendicular to x axis) per unit time. C is the number density (concentration), i.e. number of particles per unit volume. The constant of proportionality, D, is the diffusion coefficient or diffusivity.

This can be generalized
to three dimensions in a straightforward manner as:

$$\boldsymbol{J} = -D\boldsymbol{\nabla}C \tag{2.2}$$

where the vector of diffusion flux, $\boldsymbol{J}$, is directed opposite to the concentration gradient vector, $\boldsymbol{\nabla}C$. Eqs. 2.1 and 2.2 give the simplest forms of Fick's first law of diffusion. The expression can be modified to include anisotropy, concentration dependence of D, external fields, and high-diffusivity paths.In this thesis, we have assumed this simplest case.

Fick's Second Law (Diffusion Equation)

In most diffusion processes, the number of particles is conserved, i.e., the particles are not reacting to form new particles or change their form. Under this assumption, we can write

the in-flux and out-flux and implementing the continuity constraints, we get the following equation:

$$-\boldsymbol{\nabla} \cdot \boldsymbol{J} = \frac{\partial C}{\partial t} \tag{2.3}$$

From Eq. 2.2 and 2.3, we get the following relation, which is Fick's second law of diffusion, also called the *diffusion equation*:

$$\frac{\partial C}{\partial t} = \boldsymbol{\nabla} \cdot (D\boldsymbol{\nabla} C) \tag{2.4}$$

Here, the $\frac{\partial C}{\partial t}$ term tells the rate at which the concentration of the particles is changing and the vector $(D\boldsymbol{\nabla} C)$ controls the magnitude of the spatial variation in the concentration in different directions. The dot product with the gradient operator, $\boldsymbol{\nabla}$, finally gives the total magnitude of change in concentration.

2.1.2 Jump Frequency, Flux and Diffusivity

Considering the diffusion of particles in solids as random walks, in which an atom jumps from one site to another, we can express the diffusion in terms of the frequency of these jumps. For a standard solid, by assuming that atoms jump to nearest neighbours, we fix the length of these jumps, which is of the order of the lattice parameters of the crystal. Using a simplistic model of unidirectional diffusion of interstitial atoms in a simple crystal, Mehrer [29], in his book *Diffusion in Solids*, has derived a relation between the flux of atoms, J, and the and the jump frequency of the atoms, Γ,

$$J = -\lambda^2 \Gamma \frac{\partial C}{\partial x} \tag{2.5}$$

Here, λ is the fixed jump length and Γ is the jump rate or jump frequency (per unit time).

Comparing this with Fick's first law, we get,

$$D = \lambda^2 \Gamma \tag{2.6}$$

This result has been obtained for a unidirectional flow. Extending this for all the six

directions (3 dimensions $\times 2$ directions), we get the total jump frequency as:

$$\Gamma_{total} = 6\Gamma \tag{2.7}$$

Thus the final relation between diffusivity and jump frequency for a simple cubic crystal is given by:

$$D = \frac{1}{6}\Gamma_{total}\lambda^2 \tag{2.8}$$

These jump processes occur due to thermal activation and can be represented by the Arrhenius equation, given as

$$\Gamma_{total} = \nu_0 \exp\left(\frac{-E_a}{k_B T}\right) \tag{2.9}$$

Here, ν_0 denotes the attempt frequency which is of the order of the Debye frequency of the lattice (generally, $10^{13} s^{-1}$), E_a is the activation energy for the ion transport, k_B is the Boltzmann constant and T is the absolute temperature. Using Eq. 2.8 and 2.9, we get the following relation, which has been used later to find diffusivities of halide ions at different temperatures.

$$D = \frac{1}{6}\lambda^2\nu_0 \exp\left(\frac{-E_a}{k_B T}\right) \tag{2.10}$$

Having established the basic theory of ion diffusion, I will now move on to the theory used to solve Hamiltonians of systems of many interacting particles.

2.2 Solving the many-body Hamiltonian

Let us consider a system of N atoms, each one with equal number of electrons. To simplify the system, divide it into ions and (valence) electrons, where ions comprise of the nucleus and core electrons. Let the total number of valence electrons in the system be n[1]. The Hamiltonian of the system is given by:

$$H = -\sum_{I=1}^{N}\frac{\hbar^2}{2M_I}\nabla_I^2 - \sum_{i=1}^{n}\frac{\hbar^2}{2m_i}\nabla_i^2 + \frac{1}{2}\sum_{I\neq J}^{N}\frac{Z_I Z_J e^2}{|R_I - R_J|} + \sum_{I=1,i=1}^{N,n}\frac{Z_I e^2}{|R_I - r_i|} + \frac{1}{2}\sum_{i\neq j}^{n}\frac{e^2}{|r_i - r_j|} \tag{2.11}$$

[1]If the number of valence electrons per atom is v, then the total number of valence electrons in the system, $n = v * N$.

where uppercase subscripts correspond to ions and lowercase subscripts correspond to electrons. The first two terms describe the kinetic energy if ions and electrons respectively. The last three terms are Coulomb potential energy of ion-ion, ion-electron and electron-electron interaction respectively.

Putting this Hamiltonian in the Schrödinger equation, $H\Psi = E\Psi$, we obtain a coupled differential equation which is impossible to solve analytically. Hence, we need to make certain approximations and try to solve it numerically.

Let us represent the above equation by the following shortened notation, for simplicity's sake.

$$H = \underbrace{T_i}_{\text{K.E. of ions}} + \underbrace{T_e}_{\text{K.E. of electrons}} + \underbrace{V_{ii}}_{\text{ion-ion interaction}} + \underbrace{V_{ie}}_{\text{ion-elec interaction}} + \underbrace{V_{ee}}_{\text{elec-elec interaction}}$$

where the meaning of each term has been described under it. We will use this notation in the subsequent sections. Let us now look at various approximations that help us simplify this equation further so that it can be solved numerically.

2.2.1 Born-Oppenheimer approximation

The mass of ions (M_I) is much larger than the mass of electron (m_i) [$M_I/m_i > 1.8 \times 10^3$]. As a result, the motion of ions with respect to that of electrons is negligible, i.e., for electrons, the ions are fixed and can be treated at static entities for the purpose of relaxing the electrons to an equilibrium position. This allows us to divide the Hamiltonian into ionic and electronic part (Hence, we can de-couple the ionic and electronic parts of the Schrödinger equation (see Eq. 2.12). This is called the Born-Oppenheimer or adiabatic approximation. Hence, we can de-couple the ionic and electronic parts of the Schrödinger equation.

$$H_{ion} = T_i + V_{ii} \tag{2.12}$$

$$H_{electron} = T_e + V_{ee} + V_{ie} + E_{ii} \tag{2.13}$$

where $V_{ie} + E_{ii}$ is treated as the effective external potential, V_{eff}, that the electrons

are subjected to as a result of the positions of ions. E_{ii} is obtained by solving the ionic Hamiltonian using the following wavefunction:

$$\Psi_{tot}(R, r) = \psi_{ion}(R) \cdot \psi_{elec}(r, R)$$

The effective Schrödinger equation now becomes:

$$[T_e + V_{ee} + V_{eff}]\psi_{elec} = E_{tot}\psi_{elec} \tag{2.14}$$

where $V_{eff} = V_{ie} + E_{ii}$ and E_{tot} is the total ground state energy of the system.

This equation needs to be further simplified before it can be solved since it still has electron-electron interaction which gives rise to a complicated electron wavefunction, ψ_{elec}. To simplify this problem, Hartree gave another approximation.

2.2.2 Hartree and Hartree-Fock Approximations

Hartree proposed that assuming no interaction between electrons, we can represent the total electron wavefunction as a product of wavefunctions of n individual electrons:

$$\psi_{elec} = \phi_1(r_1) \cdot \phi_1(r_2) \cdot ... \cdot \phi_n(r_n) \tag{2.15}$$

where $\phi_i(r_i)$ is the wavefunction of the i^{th} electron. Hence, after putting this wavefunction into Eq. 2.14, we get n independent equations for all the electrons given by:

$$[T_e(r_i) + V_{eff}(r_i) + V_{ee}(r_i)]\phi_i(r) = \epsilon_i\phi_i(r) \tag{2.16}$$

where ϵ_i is the energy of the i^{th} electron. Expanding this notation and operating the Hamiltonian onto the wavefunction, we get the following equation:

$$-\frac{\hbar^2}{2m_i}\nabla_i^2\phi_i(r) + V_{eff}(r_i)\phi_i(r) + \underbrace{\frac{e^2}{2}\int \frac{\sum_{i\neq j}|\phi_j(r')|^2}{|r-r'|}dr'\phi_i(r)}_{V_{ee}(r_i)} = \epsilon_i\phi_i(r) \tag{2.17}$$

This is the **Hartree** equation. The total energy of the system is given by $E = \sum_i \epsilon_i$. The

V_{ee} term in this equation represents the mean Coulomb potential field experienced by the electron (whose wavefunction is $\phi_i(r)$). This approximation reduces the number of variables to a great extent, hence reducing the complexity of the equation.

However, this assumption has a fundamental problem. Representing the wavefunction as merely a product of individual electron wavefunctions does not account for the Pauli exclusion principle, which states that there can be no two electrons with the same set of quantum numbers in the same position. This comes from the Fermi-Dirac statistics for electrons. This has been rectified by the **Hartree-Fock** approximation where the wavefunction is given by the Slater determinant. This is now an anti-symmetric wavefunction. This accounts for the energy due to exchange interactions between the electrons.

$$\psi_{elec} = \frac{1}{\sqrt{n!}} \begin{vmatrix} \phi_1(r_1) & \phi_2(r_1) & \cdots & \phi_n(r_1) \\ \phi_1(r_2) & \phi_2(r_2) & \cdots & \phi_n(r_2) \\ \vdots & \vdots & \ddots & \vdots \\ \phi_1(r_n) & \phi_2(r_n) & \cdots & \phi_n(r_n) \end{vmatrix}$$

Putting this wavefunction in Eq. 2.14, we get the following equation:

$$[T_e(r_i) + V_{eff}(r_i) + V_{ee}(r_i, r_{i'})]\phi_i(r) = \epsilon_i \phi_i(r) \tag{2.18}$$

Expanding this notation and operating the Hamiltonian onto the wavefunction, we get the Hartree-Fock equation:

$$-\frac{\hbar^2}{2m_i}\nabla_i^2\phi_i(r) + V_{eff}(r_i)\phi_i(r) + \underbrace{\overbrace{e^2 \int \frac{\sum_{i\neq j}|\phi_j(r')|^2}{|r-r'|}dr'\phi_i(r)}^{\text{Coulomb interaction}} - \overbrace{e^2\sum_{i\neq j}\int \frac{\phi_i^*(r)\phi_j(r')}{|r-r'|}dr'\phi_i(r)}^{\text{Exchange interaction}}}_{V_{ee}(r_i)} = \epsilon_i\phi_i(r) \tag{2.19}$$

Notice that this equation has an extra term due to interaction between electrons. This is because of the asymmetric wavefunction which gives rise to the exchange interaction between the electrons.

The Hartree-Fock equation converts the many-particle Schrödinger equation into a set of single particle equations and the final energy can be obtained by adding all the individual energies. This is significant progress so far, however, we still have a large number of equations[2]. This would require large amount of computing power, which is not feasible.

Apart from this technical problem, there is a physical problem with this equation as well. The kinetic energy written in this equation is for a system of non-interacting particles. However, we know that our system has interacting particles. It is still unknown how to write the kinetic energy for a system of interacting particles.

This is where Density Functional Theory comes into picture. In DFT, we use charge density ($|\Psi|^2$) as the fundamental quantity instead of wavefunction (Ψ), which further reduces the degrees of freedom, and hence, the number of equations. This theory also takes care of the kinetic energy of the interacting system, addressed by the Kohn-Sham scheme discussed in section 2.3.2.

2.3 Density Functional Theory

Density Functional Theory allows us to obtain properties of systems based on their ground state charge density ρ_0. This reduces the degrees of freedom of the Hamiltonian from $3\mathcal{N}$ to $\mathcal{N}$, where $\mathcal{N}$ is the total number of particles in the system. The basis of this theory can be understood by two important theorems given by Hohenberg and Kohn.

In the following sections, these theorems have been discussed and then applied to the Hamiltoninan given in Eq. 2.19. It can be represented in short-hand notation in the following way:

$$H = T_e + E_{ii} + \sum_i V_{ext}(r_i) + E_x \tag{2.20}$$

Here, $E_{ii} = V_{eff}(r_i)\phi_i(r)$, is a constant additive term to the potential energy, $\sum_i V_{ext}(r_i) = e^2 \int \frac{\sum_{i\neq j} |\phi_j(r')|^2}{|r-r'|} dr'$, is the net external potential experienced by each electron due to all the other electrons and $E_x = -e^2 \sum_{i\neq j} \int \frac{\phi_i^*(r)\phi_j(r')}{|r-r'|} dr'$, is the exchange interaction of electrons.

[2]Number of equations = number of electrons in the system (n). And for a system with 10^{23} atoms (1 mole of a substance), with v valence electrons on each atom, we will have $n = v * 10^{23}$ number of equations.

2.3.1 Hohenberg-Kohn Theorems

Theorem 1

For any system of interacting particles in an external potential $\mathbf{V_{ext}}$, the external potential $\mathbf{V_{ext}}$ can be uniquely determined, except for an additive constant, by the ground state density $\rho_{\mathbf{0}}(\mathbf{r})$ of the interacting particles.

Theorem 2

For a system of interacting particles in any external potential, $\mathbf{V_{ext}}$, there exists a universal energy functional $\mathbf{E}[\rho(\mathbf{r})]$ where $\rho(\mathbf{r})$ is the charge density of interacting particles. For any particular $\mathbf{V_{ext}}$, the global minimum of $\mathbf{E}[\rho(\mathbf{r})]$ gives the ground state energy $\mathbf{E_0}$ of the system and the charge density corresponding to this global minimum is the ground state charge density, $\rho_{\mathbf{0}}(\mathbf{r})$, of the interacting particles.

Theorem 1 establishes a one-to-one correspondence between V_{ext} and $\rho_0(r)$, which means that a system of interacting particles is uniquely determined by its ground state charge density. Theorem 2 conveys that the minimisation of the energy functional, $E[\rho(r)]$, with respect to the charge density, $\rho(r)$, gives us the ground state energy and corresponding charge density, which can be used to find all other properties of the system.

Therefore, we can represent our Hamiltonian, given in Eq.2.20, in terms of charge density.

$$E[\rho(r)] = T_e[\rho(r)] + \int V_{ext}(r)\rho(r)dr + E_x(\rho(r)) + E_{ii}. \tag{2.21}$$

2.3.2 Kohn-Sham Scheme

In the Kohn-Sham scheme, a system of interacting particles [A(ρ_A)] is mapped on to a system of non interacting particles [A'(ρ_A)], with an additional correction term, keeping the same ground state charge density (ρ_A).

Under this scheme, the Hamiltonian of interacting electrons can be simplified to a Hamil-

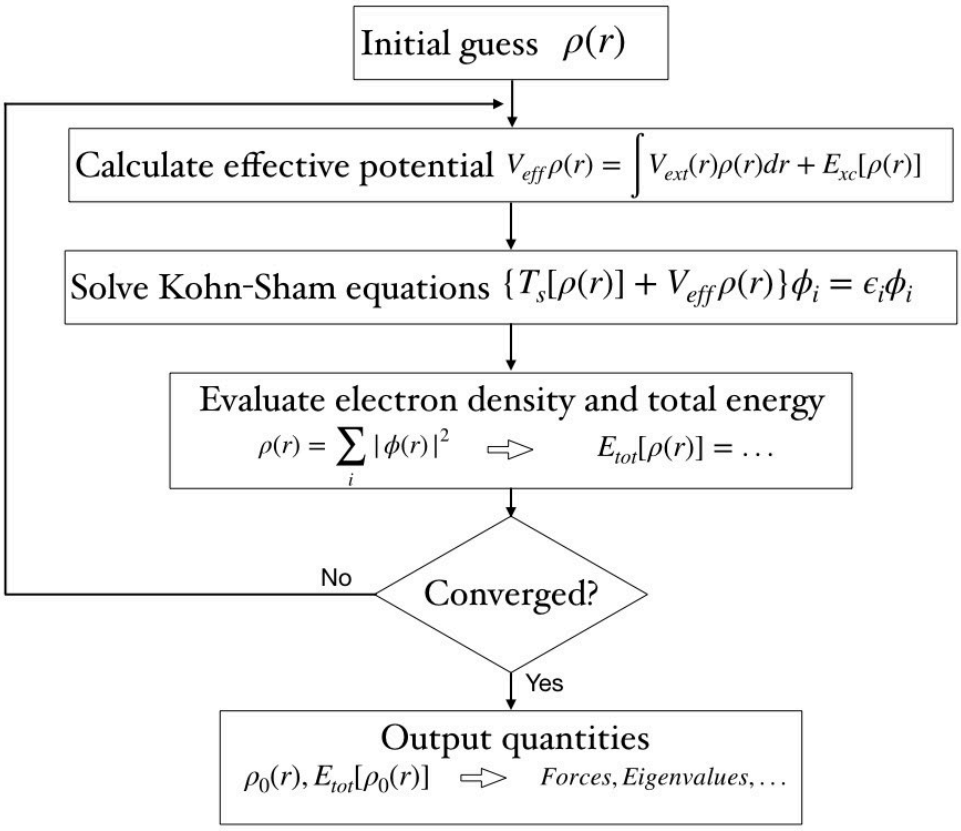

Figure 2.1: Block diagram of the Kohn-Sham scheme.

tonian of non interacting electrons which experience a net mean field due to all other electrons. We have already expressed the electron-electron interaction in this manner, however, the kinetic energy has not been looked into. The kinetic energy term in Eq. 2.21 is the kinetic energy of interacting electrons. Therefore, we need to represent the kinetic energy as the sum of $T_{\text{non-interacting}}$ and some error δT. This error is called the **correlation-kinetic energy** of interacting electrons.

The final ground state energy that we get is represented as:

$$E_{KS}[\rho(r)] = T_s[\rho(r)] + \int V_{ext}(r)\rho(r)dr + E_x(\rho(r)) + E_c(\rho(r)) + E_{ii}. \tag{2.22}$$

here, T_s is the kinetic energy of non-interacting electrons, E_c is the correlation energy. We can club E_x and E_c to write it as E_{xc}, which is called the **exchange-correlation energy**.

Applying variational principle, the above energy functional is minimized with respect to the single particle wave functions $\phi_i(r)$, to obtain the ground state properties in a self-consistent manner. The self consistent Kohn-Sham equations are given by plugging this Hamiltonian into the Schrödinger equation.

$$\{T_s[\rho(r)] + \int V_{ext}(r)\rho(r)dr + E_x(\rho(r)) + E_c(\rho(r)) + E_{ii}\}\phi_i(r) = \epsilon_i\phi_i(r) \tag{2.23}$$

By using the self-consistent iterative method given in Fig. 2.1, we arrive at the ground state energy of the system. Note that the single particle wave functions in Kohn-Sham equations do not represent the actual electronic wave functions. But they are important in obtaining the charge density in the self-consistent loops (using the relation $\rho(r) = \sum_i |\phi_i(r)|^2$).

2.4 Exchange-Correlation Functionals

As we have seen in the previous sections, the exchange-correlation energy arises from the interaction between electrons and can only be approximated up to a limit. All of DFT calculations, therefore, boil down to how well one has approximated the exchange-correlation functional, $E_{xc}[\rho]$. There are several approaches one can take depending on the system in question.

2.4.1 Local Density Approximation (LDA)

Within LDA, the $E_{xc}[\rho]$ is written as a function of charge density at a local point and the electron charge density is considered as a homogeneous density function throughout the system. It is given by the following relation:

$$E_{xc}^{LDA}[\rho] = \int \rho(r)E_{xc}^{homo}(\rho(r))dr \tag{2.24}$$

where E_{xc}^{homo} is the exchangecorrelation energy for homogeneous electron density.

2.4.2 Generalised Gradient Approximation (GGA)

In the GGA approach, the $E_{xc}[\rho]$ is considered as a function of not only the charge density but also the gradient of charge density.

$$E_{xc}^{GGA}[\rho] = \int \rho(r) E_{xc}(\rho(r)) dr + \int F_{xc}(\rho(r), \nabla\rho(r)) dr \tag{2.25}$$

The additional exchange contribution from the enhancement factor, F_{xc} results in higher exchange energies than LDA for high and moderate electronic densities, which is consistent with the fact that exchange interaction dominates over correlation for the above density regimes.

2.4.3 Hybrid Functionals

Typically, the exchange correlation functional of DFT is mixed with partial exchange contribution from Hartree-Fock method. The Hyde-Scuseria-Ernzerhof hybrid functional (HSE06) involves separation of the short range Hartree-Fock exchange and a rapid screening of the long range Hartree-Fock exchange terms [14]. Further, only 1/4th short-range Hartree-Fock exchange is mixed with the 3/4th shortrange DFT exchange.

$$E_{xc}^{HSE} = \frac{1}{4} E_{xc}^{HF(short)} + \frac{3}{4} E_{xc}^{DFT(short)} + E_{x}^{DFT(long)} + E_{c}^{DFT} \tag{2.26}$$

2.5 Nudged Elastic Band (NEB) Method

The nudged elastic band is a method to find saddle points and minimum energy pathway (MEP) between known initial and final states. It starts with the creation of equally spaced images through a linear interpolation scheme in-between the two states. All the images are then optimised to reach their minimum possible energy while maintaining equal distances between the neighbouring images.

The images are prevented to relax to their ground state energies (as would be the case

with normal DFT minimisation) by applying only a part of the force. This is ensured by adding spring forces between the images along the "elastic band" which connects them. There is an additional force acting perpendicular to the MEP which pulls the image towards it [3].

The following graph illustrates this process of optimising an image quite well.

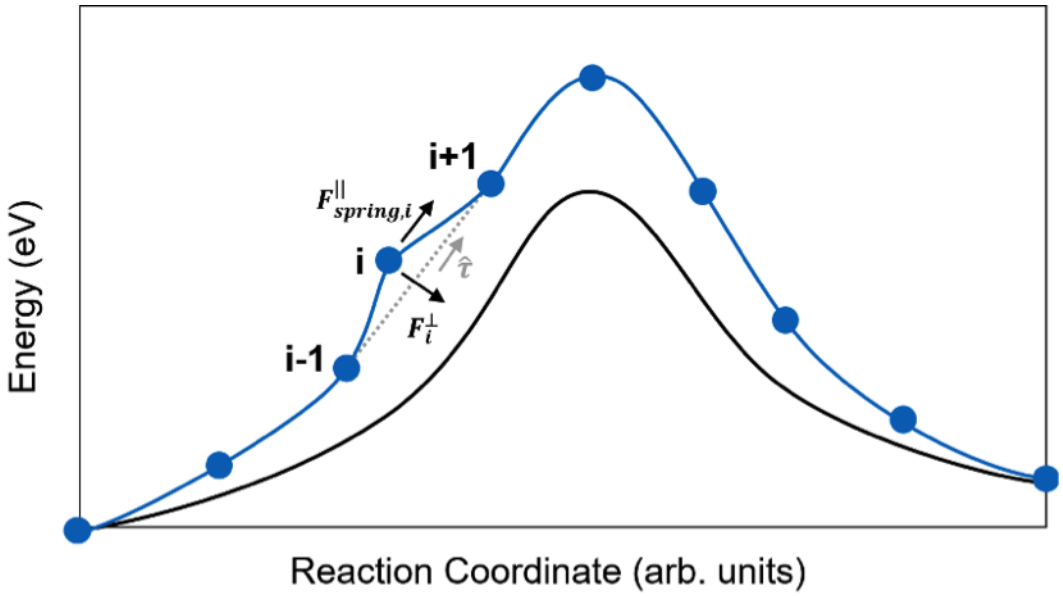

Figure 2.2: The NEB method: only the components of force on the i^{th} image that are acting parallel and perpendicular to the MEP is considered while minimisation of the energy functional of the said image. Here the blue line is the linearly interpolated pathway and the black line is the MEP. Figure reproduced from [11] with permission.

2.6 Computational Details

The work presented in this thesis has been carried out using Vienna ab initio Simulation Package (VASP)[26][25]. The structural and electronic properties of the systems were calculated using Density Functional Theory with the Generalised Gradient Approximation (GGA) using the Perdew-Burke-Ernzerhof (PBE)[39] exchange-correlation functional, along with spin-orbit coupling. The unit cells were fully relaxed until all the forces became smaller than 0.005 eV/Å threshold energy. Since PBE+SO underestimates the band gap, the band

[3]Since in this process all the images are being optimised simultaneously, it is always better to assign the number of processors as a multiple of the number of images for NEB calculations.

structures were recalculated using the Heyd-Scuseria-Ernzerhof hybrid exchange correlation functional (HSE06). All the calculations were performed within the projector augmented wave (PAW) formalism[4] and the wave functions were expanded in a plane-wave basis with 400 eV kinetic energy cut-off. The Brillouin zone sampling using the Monkhorst-Pack k grids [33]. Details for each phase are provided in Table 2.1.

Phase	**K-mesh for optimisation**	
	Unitcell	**Supercell**
Cubic	4x4x4	2x2x4
Tetragonal	7x7x5	3x3x2
Orthorhombic	7x7x5 (5x5x7)	3x3x2

Table 2.1: K-mesh for unit cell and supercell optimisation of different structures.The values in the bracket are for X = Cl^-. Since the orthorhombic $CsPbCl_3$ has higher symmetry than the other two along z-axis, the number of atoms is lesser in that direction for this crystal. Hence, the Brillouin zone changes accordingly.

Thereafter, activation energies for ion diffusion in the perovskites was calculated using the Cl-NEB method[13]. Supercells with 160 atoms were created for all the systems and optimised using PBE functional. Thereafter, two copies were made with a halide vacancy in each one, making sure that they are nearest neighbour vacancies. These structures with vacancies, after being optimised, were used as initial and final structures for conducting NEB calculations.

Chapter 3

Results and Discussion

In this chapter, I have presented the results of this thesis. In the first two sections, 3.1 and 3.2, I have discussed the structural and electronic properties of the systems in focus and the trends in their properties have been elaborated upon. They have been compared with previous works, both experimental and theoretical. In section 3.3, I have presented the formation energy and activation energy for vacancy formation and transport respectively. Results for cubic and orthorhombic phase have been compared for different halide perovskites. Lastly, the results for cubic phase have been compared with available experimental data. I have concluded this chapter with a comment on the implications of these energy values for different halide perovskites.

3.1 Structural Properties

The structural properties of $CsPbX_3$ have been obtained before both experimentally and theoretically. Here, we have calculated the same using PBE functional and compared it to previous results. Original .cif files for most[1] of the structures were taken from Materials Project [20].

[1]For tetragonal $CsPbI_3$, I used the tetragonal $CsPbBr_3$ structure and replaced Br with I. Orthorhombic $CsPbI_3$ .cif file was taken from [47]

Material	Phase	Calculated (Å)	Experimental (Å)	Others (Å)
$CsPbCl_3$	cubic	a = 5.719	a = 5.605[32]	a = 5.729[10]
	orthorhombic	a = 7.948 b = 7.948 c = 5.780	- - -	- - -
$CsPbBr_3$	cubic	a = 5.972	5.874[32]	a = 6.005 [2]
	tetragonal	a = b = 8.433 c = 11.991	a = b = 8.48 c = 15.25 [2]	a = b = 7.978 c = 14.640 [2]
	orthorhombic	a = 8.420 b = 11.948 c = 8.303	a = 8.244 b = 11.735 c = 8.198 [46]	a = 8.251 b = 11.751 c = 8.169 [2]
$CsPbI_3$	cubic	a = 6.352	a = 6.289[44]	a = 6.050[5]
	tetragonal	a = b = 8.984 c = 12.801	- -	- -
	orthorhombic	a = 9.053 b = 8.777 c = 12.674	a = 8.856 b =8.576 c =12.472[47]	- - -

Table 3.1: Lattice parameters are calculated using the PBE functional.

As discussed in chapter 1, the structure of perovskites is made up of eight BX_6 octahedrons and cation A sitting in the centre of these octahedra. The lattice parameters of $CsPbX_3$ increase in magnitude from Cl to Br to I for all the phases, as expected, because the size of the halide increases in that order.

It is to be noticed that the volume of orthorhombic $CsPbCl_3$ is less than half of the other two. This is because the number of atoms in its unit cell is also half of the number in the other two. $CsPbCl_3$ has higher symmetry as compared to $CsPbBr_3$ and $CsPbI_3$, most probably because of the smaller size of Cl ion. This results in reduction of the unit cell by half. However, there are .cif files available which have not considered the two halves of the cell as symmetric. I realsied this fact much later and so did not use the other structure.

3.2 Electronic Properties

The band structures of all the crystal systems were calculated using PBE functional, and recalculated by adding spin-obit coupling effect and then using HSE06 hybrid functional. The results have been compared with experimental data and previous theoretical results.

Material	Phase	Calculated (eV)			Exp.(eV)	Others (eV)
		PBE	PBE+SO	HSE+SO		
$CsPbCl_3$	cubic	2.18	1.11		2.82[41]	2.50 (GGA)[22]
	orthorhombic	2.35	1.43	2.13	-	2.33 (GGA)[2]
$CsPbBr_3$	cubic	1.74	0.69		2.00[41]	1.42 (LDA)[5]
	tetragonal	1.82	0.64		-	0.79 (GGA)[2]
	orthorhombic	2.03	1.12	1.67	2.24[46]	1.80 (GGA)[22]
$CsPbI_3$	cubic	1.44	0.34		1.44[41]	1.32 (GGA)[22]
	tetragonal	1.53	0.51		-	-
	orthorhombic	1.76	0.84	1.29	1.72[54]	1.70 (GGA)[52]

Table 3.2: $CsPbX_3$ systems have direct band gaps in all the three phases. PBE+SOC heavily underestimates the band gaps. Hence, the HSE06+SOC functional was used to recalculate their band structures.

It seems that PBE functional gives results closer to the expected value but that is due to numerical errors canceling out. If we consider spin-orbit coupling (and it is important that we do, because spin-orbit coupling has significant effects on energy levels of these materials due to Pb^{+2} ion) with the PBE functional, it is observed that the band gaps are heavily underestimated. Therefore, a different approximation method is required for lead halide perovskites. We used the HSE06 functional with spin orbit coupling to recalculate the band structures[2].

It is observed that the band gap increases when we go from bigger to smaller halide ion, i.e., $E_{I^-} < E_{Br^-} < E_{Cl^-}$. Comparing the phases, we find that the band gap increases with the increase in the distortion of PX_6 octahedrons in the perovskite lattice, i.e., $E_{\text{cubic}} < E_{\text{tetragonal}} < E_{\text{orthorhombic}}$.

3.3 Vacancy/ion migration energy

The nearest neighbour vacancy structures, say vacancy 1 and vacancy 2, were used as initial and final structures for NEB calculations. Here, we have provided the activation barriers for halide ion migration along a given path and discussed how they vary with different halide

[2]The calculation with HSE+SO are still going on since they are quite computationally heavy.

ions, different phases and theoretical approximations. Results have been compared with experimental values as well. The path for cubic phase of $CsPbBr_3$ has been shown in fig. 3.1.

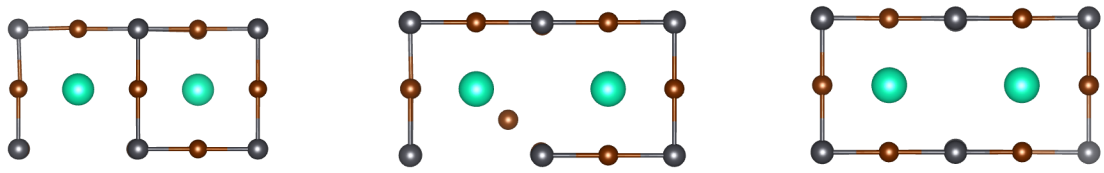

Initial state Transition state Final state

Figure 3.1: The path followed by Br^- ion in cubic $CsPbBr_3$.The given figures are in the a-c plane. The green atom is Cs, black is Pb and brown is Br.

3.3.1 Vacancy formation energy

Supercells (pristine) of $CsPbX_3$ systems were created to get 160 atoms per cell. After their optimization using PBE functional, two separate structures (defective) with nearest neighbour halide vacancies were generated. For all the structures, we have calculated the energy required to form a vacancy (vacancy formation energy, E_v) by optimising both the pristine and defective supercells and comparing their ground state energies (E_0).

Material	**Phase**	**E_0 (eV)**		**E_v (eV)**
		Pristine	**Defective**	
$CsPbCl_3$	cubic	-564.145	-560.441	3.704
	orthorhombic	-565.338	-560.365	5.193
$CsPbBr_3$	cubic	-510.105	-505.791	4.314
	tetragonal	-511.019	-507.001	4.018
	orthorhombic	-512.493	-507.965	4.528
$CsPbI_3$	cubic	-451.103	-447.495	3.609
	tetragonal	-452.444	-448.858	3.586
	orthorhombic	-454.522	-450.748	3.774

Table 3.3: Vacancy formation energies for $CsPbX_3$ in different phases.

The vacancy formation energy for cubic phase is lower than that of orthorhombic phase for all the halides. Additionally, the formation energy of tetragonal phases of $CsPbBr_3$ and

$CsPbI_3$ is the lowest of the three phases. This needs to be verified by experimental studies. Since we have used the PBE functional and not included spin-orbit effects while optimising these supercells, our results need some improvement. But doing these calculations for a supercell of 160 atoms is quite a heavy job. Therefore, better and faster computational methods need to be incorporated to analyse these systems with better accuracy.

3.3.2 Activation Energy and Diffusivity

The structures of tetragonal phase with the vacancy defect did not completely optimise and hence, the NEB data could not be obtained.

Cubic phase

The results for the cubic phase have been analysed in detail in this subsection.

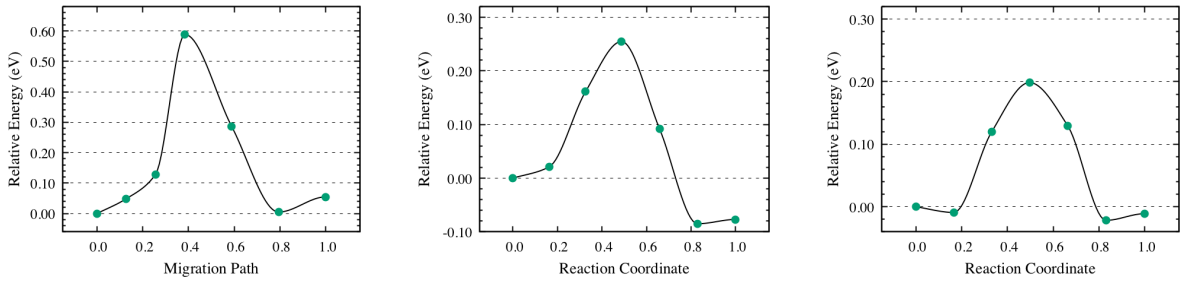

Figure 3.2: Energy barriers for (a) Cl^-, (b) Br^- and (c) I^- ions in cubic phase are calculated as 0.59 eV, 0.25 eV and 0.20 eV respectively.

(a) The value of activation barrier for Cl ion is much higher than the expected experimental value (0.29 eV). It also shows a peculiar bump in the NEB graph and is highly asymmetric in nature. Our guess is that there is some problem with the .cif file. This calculation needs to be redone from scratch using a different initial structure.

(b) The value of activation barrier for Br is in agreement with the experimental value. However, the difference in energies of the initial and final structures needs to be looked at. In fact, this is the case with most of my vacancy supercells. This is being addressed by reversing the initial and final structure order and redoing the NEB calculation.

(c) The NEB graph for I ion is quite symmetric. However, the first and fifth images have lower energies than the zeroth (initial) and sixth (final) images. This is because these structures did not converge completely (forces were of the order of 0.045 eV). The barriers is being recalculated by giving the first and fifth images as the initial and final images in the NEB calculation.

Orthorhombic phase

Here, we present the activation energy barrier for orthorhombic phases of $CsPbX_3$ (X = Cl, Br, I). It is observed that the activation energy for Cl^- is the highest, followed by I^- and then Br^-. Since Cl^- has a smaller size, and is more tightly packed, it would form stronger

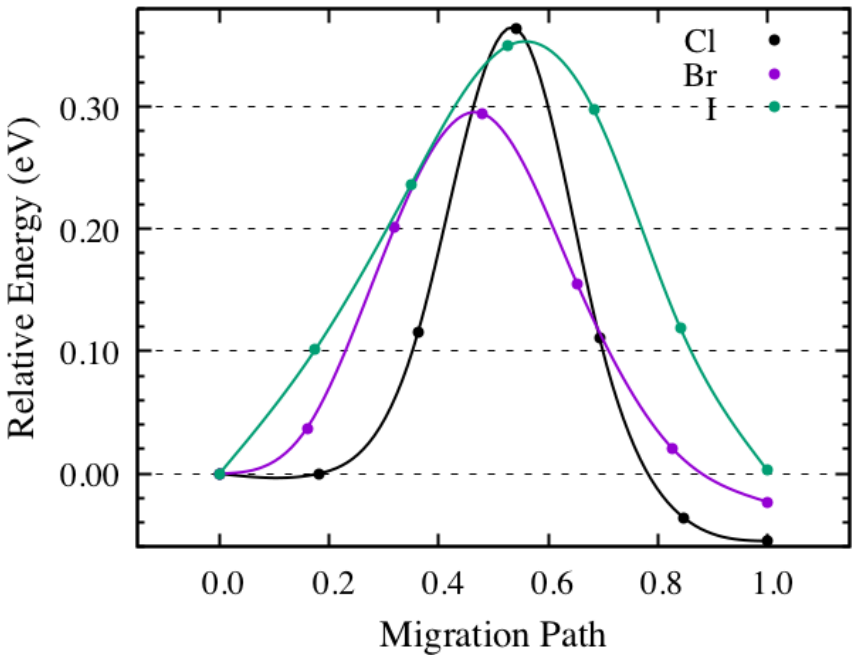

Figure 3.3: Energy barriers for (a) Cl^-, (b) Br^- and (c) I^- ions in orthorhombic phase are calculated as 0.36 eV, 0.30 eV and 0.35 eV respectively.

bonds with the neighbouring atoms. Hence, it is expected to have the highest energy barrier for transporting. By this logic, Br^- should be in the middle and I^- should have the lowest barrier. However, our results differ from this hypothesis. If we assume that our theoretical methods are accurate and do not require further improvement, then one physical reason for this trend could be that apart from tight bonding, size also plays a role in moving through a

medium. It would be more difficult for a larger atom to transport because of its heavy mass. Hence, these two terms, extent of bonding and mass, compete with each other to give E_a of an ion.

Using equation 2.10, which gives the relation between diffusivity, activation energy, migration path length and temperature, we have calculated the diffusivity of halide ions in orthorhombic phase at different temperatures, plotted in fig 3.4.

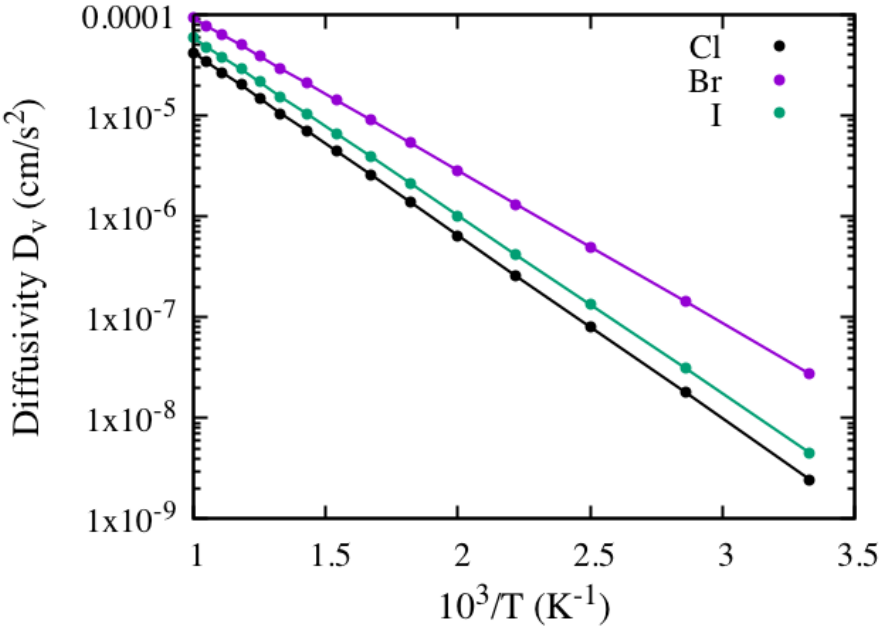

Figure 3.4: Diffusivity of halide ions in orthorhombic phase of $CsPbX_3$ is plotted with temperature. The values of path length, λ, for Cl, Br and I are 4.07 Å, 4.25 Å, 4.55 Årespectively and the attempt frequency, ν_0 is taken as $10^{13}s^{-1}$.

The diffusivity of Cl is found to be lowest and that of Br, the highest. The reasoning given for activation energies can be extended to diffusivity as well.

Formation and activation energy - is there any trend?

Although there is no analytical proof for this fact but it has been empirically established that the activation energy is directly proportional to the formation energy of a reaction. This was first proposed by Bronsted-Evans-Polanyi [3]. Kabir et. al. [23] have analysed the trend between activation energy and formation energy of various diffusion reactions and have

shown a linear relation between the formation and activation energies. We have plotted our values of E_a and E_v which is shown in Fig. 3.5. Except for cubic $CsPbCl_3$ and orthogonal

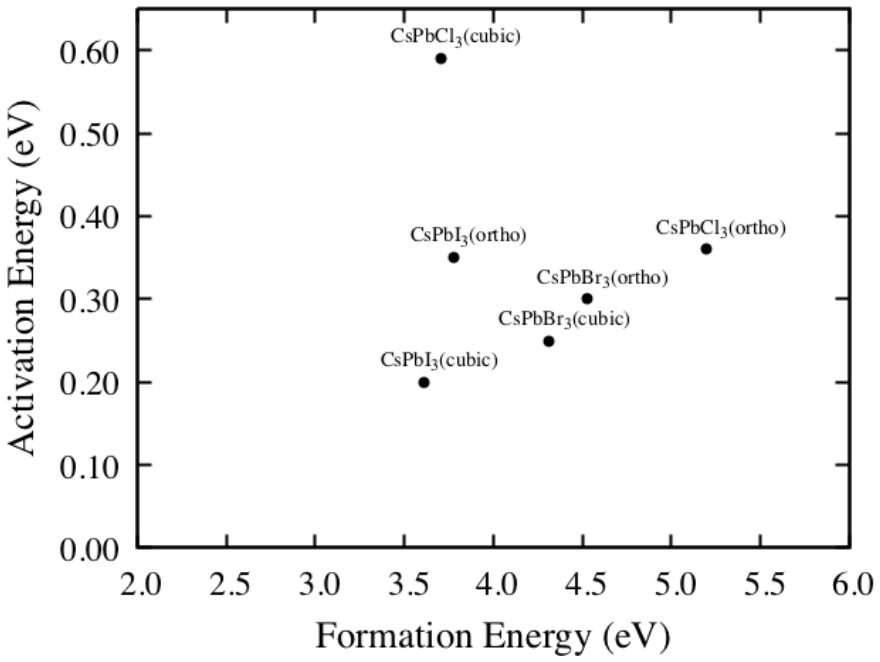

Figure 3.5: Activation energy and formation energies of each structure has been plotted to check if there is any trend followed.

$CsPbI_3$, the structures follow more or less a Bronsted-Evans-Polanyi correlation.

3.3.3 Comparison with experimental results

There are a few experimental papers which have discussed ion transport in Cs based halide perovskites. It has been experimentally found that E_a of halide ions in cubic phases of $CsPbCl_3$ and $CsPbBr_3$ is 0.29eV and 0.25eV respectively[31]. The experimental values were obtained using Tubandt, EMF and ion-blocking methods at temperature ranges from 150 °C to the melting point of the structures. Our calculated value for $CsPbBr_3$ is in agreement with the experimental value. However, the value for $CsPbCl_3$ is way off, most probably because of theoretical errors, that are being resolved at the moment.

There was another experimental study in which the value of activation energy for (Br/Cl) ion diffusion was found out to be 0.44 ± 0.02 eV for a structure of single crystals of $CsPbBr_3$

nanowires (NWs) and cubic $CsPbCl_3$. This was obtained by physically stacking single crystal $CsPbCl_3$ microplates on single-crystal $CsPbBr_3$ NWs [37]. It is debatable whether this experimental value can be compared with the theoretical activation value for cubic $CsPbX_3$ (X = Cl, Br) since the stacking would result in some grain boundaries and the diffusion would not be just because of vacancy defects.

There have been no experimental studies of ion diffusion in orthorhombic or tetragonal structures. Our theoretical results will motivate such studies in future if we get interesting results.

Chapter 4

Conclusion and Outlook

In this work, we have studied ion transport of halide ions in $CsPbX_3$ (X = Cl, Br, I) in different crystal phases. Having better insights on the mechanism of ion transport would significantly improve our chances of developing more stable perovskites, which can be used in solar cells. Our key results include the following:

1. The formation energies of halide vacancies, E_v, in $CsPbX_3$ are in the range of 3.7 - 5.2 eV. The formation energy for cubic phase is lower than that of orthorhombic phase for all the halides. However, the formation energy of tetragonal phases of $CsPbBr_3$ and $CsPbI_3$ is the lowest of all the three phases. More calculations need to be done to conclude anything about them.

2. Comparison of activation energies between phases reveals that E_a is higher for ions in cubic than in orthorhombic phase. The results for tetragonal phase are still ongoing.

3. We have found the diffusivity of halide ions with respect to the temperature by considering the ion jump frequency as 10^{13}. It is found that the diffusivity of Br ions is the highest, followed by I and the lowest is for Cl ions. This trend has been discussed in detail in section 3.3.2.

4. The relationship between formation energy and activation energy of vacancy defects has been looked at. Most of the structures follow a linear graph but more number of data points are required to make a conclusion.

5. Finally, we have compared our results with experimental ones and found that the experimental barriers are lower than the theoretical ones. The possible reasons for that could be:

    - There is diffusion of ions due to defects other than vacancy defects, as shown in Fig. 1.4. It is extremely difficult to experimentally differentiate the activation energies due to different defects within the crystal.
    - We have used the GGA approach calculate the activation barriers. It is possible that more accurate numerical methods are required for these systems.
    - It is difficult to conclude whether the experimental phenomena is being correctly simulated in the theoretical model.

Hence, understanding ion transport in perovskites is crucial in advancement of perovskite photovoltaics. Using computational tools, one can predict favourable perovskite structures which have higher ion activation energies, and hence less ion transport, thereby reducing the chances of distortion in the crystal structure.

4.1 Future work

There are so many questions yet to be answered in this work and with each answer, a new question arises. We need to carry out several calculations before we can arrive at a concrete conclusion. Currently, some of them are being done (as mentioned above).

In this work, we have fixed the vacancy concentration for comparing ion transport mechanisms, but it would be worthwhile to analyse the activation energies at a fixed temperature for all the structures. For each temperature value, we would have a corresponding vacancy concentration in the crystal. This would allow us to determine if there is any changes in the activation energies due to vacancy defect concentration. Additionally, it would be useful to analyse how the activation barrier changes with the direction of transport. So far, we have considered isotropic conditions and similar environments around the ions. But this is not necessarily the case, especially for orthorhombic and tetragonal phases.

Bibliography

[1] Oxford pv sets world record for perovskite solar cell, 25 June 2018. https://www.oxfordpv.com/news/oxford-pv-sets-world-record-perovskite-solar-cell.

[2] M. Ahmad, G. Rehman, L. Ali, M. Shafiq, R. Iqbal, R. Ahmad, T. Khan, S. Jalali-Asadabadi, M. Maqbool, and I. Ahmad. Structural, electronic and optical properties of cspbx3 (x= cl, br, i) for energy storage and hybrid solar cell applications. *Journal of Alloys and Compounds*, 705:828–839, 2017.

[3] T. Bligaard, J. K. Nørskov, S. Dahl, J. Matthiesen, C. H. Christensen, and J. Sehested. The brønsted–evans–polanyi relation and the volcano curve in heterogeneous catalysis. *Journal of Catalysis*, 224(1):206–217, 2004.

[4] P. E. Blöchl. Projector augmented-wave method. *Phys. Rev. B*, 50:17953–17979, Dec 1994.

[5] Y. Chang, C. Park, and K. Matsuishi. First-principles study of the structural and the electronic properties of the lead-halide-based inorganic-organic perovskites (ch˜ 3nh˜ 3) pbx˜ 3 and cspbx˜ 3 (x= cl, br, i). *Journal-Korean Physical Society*, 44:889–893, 2004.

[6] B. Chen, M. Yang, S. Priya, and K. Zhu. Origin of j-v hysteresis in perovskite solar cells. *The Journal of Physical Chemistry Letters*, 7(5):905–917, 2016. https://doi.org/10.1021/acs.jpclett.6b00215.

[7] J.-P. Correa-Baena, M. Saliba, T. Buonassisi, M. Grätzel, A. Abate, W. Tress, and A. Hagfeldt. Promises and challenges of perovskite solar cells. *Science*, 358(6364):739–744, 2017. http://science.sciencemag.org/content/358/6364/739.

[8] S. DAO. Why solar? the advantages of pv solar energy compared to the other renewables, 2017. https://medium.com/@solar.dao/why-solar-the-advantages-of-pv-solar-energy-compared-to-the-other-renewables-1664f82ba9fe.

[9] K. Domanski, B. Roose, T. Matsui, M. Saliba, S.-H. Turren-Cruz, J.-P. Correa-Baena, C. R. Carmona, G. Richardson, J. M. Foster, F. De Angelis, et al. Migration of cations induces reversible performance losses over day/night cycling in perovskite solar cells. *Energy & Environmental Science*, 10(2):604–613, 2017.

[10] M. Ghebouli, B. Ghebouli, and M. Fatmi. First-principles calculations on structural, elastic, electronic, optical and thermal properties of CsPbCl3 perovskite. *Physica B: Condensed Matter*, 406(9):1837–1843, apr 2011.

[11] M. Ghoussoub. First principles investigation of heterogeneous catalysis on metal oxide surfaces. http://hdl.handle.net/1807/72729.

[12] G. Grancini, C. Roldán-Carmona, I. Zimmermann, E. Mosconi, X. Lee, D. Martineau, S. Narbey, F. Oswald, F. De Angelis, M. Graetzel, and M. K. Nazeeruddin. One-Year stable perovskite solar cells by 2D/3D interface engineering. *Nature Communications*, 8:15684, Jun 2017. https://doi.org/10.1038/ncomms15684.

[13] G. Henkelman, B. P. Uberuaga, and H. Jnsson. A climbing image nudged elastic band method for finding saddle points and minimum energy paths. *The Journal of Chemical Physics*, 113(22):9901–9904, 2000.

[14] J. Heyd, G. E. Scuseria, and M. Ernzerhof. Hybrid functionals based on a screened coulomb potential. *The Journal of chemical physics*, 118(18):8207–8215, 2003.

[15] S. Hirotsu. Experimental studies of structural phase transitions in cspbcl3. *Journal of the Physical Society of Japan*, 31(2):552–560, 1971.

[16] S. Hirotsu, J. Harada, M. Iizumi, and K. Gesi. Structural phase transitions in cspbbr3. *Journal of the Physical Society of Japan*, 37(5):1393–1398, 1974.

[17] M. Höök and X. Tang. Depletion of fossil fuels and anthropogenic climate change a review. *Energy Policy*, 52:797–809, Jan 2013.

[18] Y. Hou, X. Du, S. Scheiner, D. P. McMeekin, Z. Wang, N. Li, M. S. Killian, H. Chen, M. Richter, I. Levchuk, N. Schrenker, E. Spiecker, T. Stubhan, N. A. Luechinger,

A. Hirsch, P. Schmuki, H.-P. Steinrück, R. H. Fink, M. Halik, H. J. Snaith, and C. J. Brabec. A generic interface to reduce the efficiency-stability-cost gap of perovskite solar cells. *Science*, 358(6367):1192–1197, 2017. http://science.sciencemag.org/content/358/6367/1192.

[19] T. J. Jacobsson, W. Tress, J.-P. Correa-Baena, T. Edvinsson, and A. Hagfeldt. Room temperature as a goldilocks environment for ch3nh3pbi3 perovskite solar cells: The importance of temperature on device performance. *The Journal of Physical Chemistry C*, 120(21):11382–11393, 2016.

[20] A. Jain, S. P. Ong, G. Hautier, W. Chen, W. D. Richards, S. Dacek, S. Cholia, D. Gunter, D. Skinner, G. Ceder, and K. a. Persson. The Materials Project: A materials genome approach to accelerating materials innovation. *APL Materials*, 1(1):011002, 2013.

[21] Q. Jiang, Z. Chu, P. Wang, X. Yang, H. Liu, Y. Wang, Z. Yin, J. Wu, X. Zhang, and J. You. Planar-structure perovskite solar cells with efficiency beyond 21%. *Advanced Materials*, 29(46):1703852, 2017. https://doi.org/10.1002/adma.201703852.

[22] R. A. Jishi, O. B. Ta, and A. A. Sharif. Modeling of lead halide perovskites for photovoltaic applications. *The Journal of Physical Chemistry C*, 118(49):28344–28349, 2014.

[23] M. Kabir and K. J. Van Vliet. Kinetics of topological stone–wales defect formation in single-walled carbon nanotubes. *The Journal of Physical Chemistry C*, 120(3):1989–1993, 2016.

[24] A. Kojima, K. Teshima, Y. Shirai, and T. Miyasaka. Organometal halide perovskites as visible-light sensitizers for photovoltaic cells. *Journal of the American Chemical Society*, 131(17):6050–6051, 2009. https://doi.org/10.1021/ja809598r.

[25] G. Kresse and J. Furthmüller. Efficient iterative schemes for ab initio total-energy calculations using a plane-wave basis set. *Phys. Rev. B*, 54:11169–11186, Oct 1996.

[26] G. Kresse and J. Hafner. Ab initio molecular dynamics for liquid metals. *Phys. Rev. B*, 47:558–561, Jan 1993.

[27] C. Li, X. Lu, W. Ding, L. Feng, Y. Gao, and Z. Guo. Formability of ABX_3 (X = F, Cl, Br, I) halide perovskites. *Acta Crystallographica Section B*, 64(6):702–707, Dec 2008.

[28] M. B. S. H. J. Liu, Mingzhen Johnston. Efficient planar heterojunction perovskite solar cells by vapour deposition. *Nature*, 501:395, September 2013.

[29] H. Mehrer. *Diffusion in Solids: Fundamentals, Methods, Materials, Diffusion-Controlled Processes*. Springer Series in Solid-State Sciences. Springer Berlin Heidelberg, 2007.

[30] L. Meng, J. You, and Y. Yang. Addressing the stability issue of perovskite solar cells for commercial applications. *Nature Communications*, 9(1):5265, 2018. `https://doi.org/10.1038/s41467-018-07255-1`.

[31] J. Mizusaki, K. Arai, and K. Fueki. Ionic conduction of the perovskite-type halides. *Solid State Ionics*, 11(3):203–211, 1983.

[32] C. K. Møller. Crystal Structure and Photoconductivity of Cæsium Plumbohalides. *Nature*, 182:1436, November 1958.

[33] H. J. Monkhorst and J. D. Pack. Special points for brillouin-zone integrations. *Phys. Rev. B*, 13:5188–5192, Jun 1976.

[34] NREL. Best research-cell efficiencies. `https://www.nrel.gov/pv/assets/pdfs/pv-efficiency-chart.20181221.pdf`.

[35] R. S. Ohl. Light-sensitive electric device, March 1941. `https://patents.google.com/patent/US2402662A/en`.

[36] R. S. Ohl. Light-sensitive electric device including silicon, March 1941. `https://patents.google.com/patent/US2443542A/en`.

[37] D. Pan, Y. Fu, J. Chen, K. J. Czech, J. C. Wright, and S. Jin. Visualization and studies of ion-diffusion kinetics in cesium lead bromide perovskite nanowires. *Nano letters*, 18(3):1807–1813, 2018.

[38] N. Pellet, J. Teuscher, J. Maier, and M. Grtzel. Transforming hybrid organic inorganic perovskites by rapid halide exchange. *Chemistry of Materials*, 27(6):2181–2188, 2015.

[39] J. P. Perdew, K. Burke, and M. Ernzerhof. Generalized gradient approximation made simple. *Phys. Rev. Lett.*, 77:3865–3868, Oct 1996.

[40] M. L. Petrus, J. Schlipf, C. Li, T. P. Gujar, N. Giesbrecht, P. Mller-Buschbaum, M. Thelakkat, T. Bein, S. Httner, and P. Docampo. Capturing the sun: A review

of the challenges and perspectives of perovskite solar cells. *Advanced Energy Materials*, 7(16):1700264, 2017. https://onlinelibrary.wiley.com/doi/abs/10.1002/aenm.201700264.

[41] L. Protesescu, S. Yakunin, M. I. Bodnarchuk, F. Krieg, R. Caputo, C. H. Hendon, R. X. Yang, A. Walsh, and M. V. Kovalenko. Nanocrystals of cesium lead halide perovskites (cspbx3, x= cl, br, and i): novel optoelectronic materials showing bright emission with wide color gamut. *Nano letters*, 15(6):3692–3696, 2015.

[42] Y. M. Y. T.-B. S. C.-C. C. H. Z. Z. H. H. Z. Y. Y. Qi Chen, Nicholas De Marco. Under the spotlight: The organicinorganic hybrid halide perovskite for optoelectronic applications. *Nano Today*, 10(3):355 – 396, 2015.

[43] Y. Rong, Y. Hu, A. Mei, H. Tan, M. I. Saidaminov, S. I. Seok, M. D. McGehee, E. H. Sargent, and H. Han. Challenges for commercializing perovskite solar cells. *Science*, 361(6408), 2018. http://science.sciencemag.org/content/361/6408/eaat8235.

[44] S. Sharma, N. Weiden, and A. Weiss. Phase diagrams of quasibinary systems of the type: Abx 3 abx 3 ; abx 3 abx 3 , and abx 3 abx 3 ; x = halogen. *Zeitschrift fr Physikalische Chemie*, 175:63–80, 01 1992.

[45] H. J. Snaith, A. Abate, J. M. Ball, G. E. Eperon, T. Leijtens, N. K. Noel, S. D. Stranks, J. T.-W. Wang, K. Wojciechowski, and W. Zhang. Anomalous hysteresis in perovskite solar cells. *J. Phys. Chem. Lett*, 5(9):1511–1515, 2014.

[46] C. C. Stoumpos, C. D. Malliakas, J. A. Peters, Z. Liu, M. Sebastian, J. Im, T. C. Chasapis, A. C. Wibowo, D. Y. Chung, A. J. Freeman, et al. Crystal growth of the perovskite semiconductor cspbbr3: a new material for high-energy radiation detection. *Crystal Growth & Design*, 13(7):2722–2727, 2013.

[47] R. J. Sutton, M. R. Filip, A. A. Haghighirad, N. Sakai, B. Wenger, F. Giustino, and H. J. Snaith. Cubic or orthorhombic? revealing the crystal structure of metastable black-phase cspbi3 by theory and experiment. *ACS Energy Letters*, 3(8):1787–1794, 2018.

[48] E. Tenuta, C. Zheng, and O. Rubel. Thermodynamic origin of instability in hybrid halide perovskites. *Scientific Reports*, 6:37654, nov 2016.

[49] W. Tress, N. Marinova, T. Moehl, S. M. Zakeeruddin, M. K. Nazeeruddin, and M. Grtzel. Understanding the rate-dependent jv hysteresis, slow time component, and aging in ch3nh3pbi3 perovskite solar cells: the role of a compensated electric field. *Energy Environ. Sci.*, 8:995–1004, 2015. http://dx.doi.org/10.1039/C4EE03664F.

[50] D. M. Trots and S. V. Myagkota. High-temperature structural evolution of caesium and rubidium triiodoplumbates. *Journal of Physics and Chemistry of Solids*, 69(10):2520–2526, 2008.

[51] H. Tsai, R. Asadpour, J.-C. Blancon, C. C. Stoumpos, O. Durand, J. W. Strzalka, B. Chen, R. Verduzco, P. M. Ajayan, S. Tretiak, et al. Light-induced lattice expansion leads to high-efficiency perovskite solar cells. *Science*, 360(6384):67–70, 2018.

[52] A. Varadwaj, P. R. Varadwaj, and K. Yamashita. Revealing the chemistry between band gap and binding energy for lead-/tin-based trihalide perovskite solar cell semiconductors. *ChemSusChem*, 11(2):449–463, 2018.

[53] P. S. Whitfield, N. Herron, W. E. Guise, K. Page, Y. Q. Cheng, I. Milas, and M. K. Crawford. Structures, Phase Transitions and Tricritical Behavior of the Hybrid Perovskite Methyl Ammonium Lead Iodide. *Scientific Reports*, 6:35685, oct 2016.

[54] Z. Yang, A. Surrente, K. Galkowski, A. Miyata, O. Portugall, R. Sutton, A. Haghighirad, H. Snaith, D. Maude, P. Plochocka, et al. Impact of the halide cage on the electronic properties of fully inorganic cesium lead halide perovskites. *ACS Energy Letters*, 2(7):1621–1627, 2017.

[55] Y. Yuan and J. Huang. Ion migration in organometal trihalide perovskite and its impact on photovoltaic efficiency and stability. *Accounts of chemical research*, 49(2):286–293, 2016.

[56] Q. Zhang, F. Hao, J. Li, Y. Zhou, Y. Wei, and H. Lin. Perovskite solar cells: must lead be replaced - and can it be done? *Science and technology of advanced materials*, 19(1):425–442, may 2018.

[57] X. Zhao and M. Wang. Organic hole-transporting materials for efficient perovskite solar cells. *Materials Today Energy*, 7, 09 2017.

[58] W. Zhou, Y. Zhao, X. Zhou, R. Fu, Q. Li, Y. Zhao, K. Liu, D. Yu, and Q. Zhao. Light-independent ionic transport in inorganic perovskite and ultrastable cs-based perovskite solar cells. *The journal of physical chemistry letters*, 8(17):4122–4128, 2017.